

Instability of Walker Propagating Domain Wall in Magnetic Nanowires

B. Hu and X.R. Wang*

Physics Department, The Hong Kong University of Science and Technology, Clear Water Bay, Kowloon, Hong Kong

(Dated: July 8, 2018)

Stability of the well-known Walker propagating domain wall (DW) solution of the Landau-Lifshitz-Gilbert equation is analytically investigated. Surprisingly, the Walker's rigid body propagating DW mode is not stable against the spin wave/wavepacket emission. In the low field region only stern spin waves are emitted while both stern and bow waves are generated under high fields. In a high enough field, but below the Walker breakdown field, the Walker solution could be convective/absolute unstable if the transverse magnetic anisotropy is larger than a critical value, corresponding to a significant modification of the DW profile and DW propagating speed.

PACS numbers: 75.60.Jk, 75.30.Ds, 75.60.Ch, 05.45.-a

Magnetic domain-wall (DW) propagation in nanowires has attracted considerable attention in recent years [1–5] because of its fundamental interest and potential applications [2, 3]. Field-driven DW dynamics is governed by the Landau-Lifshitz-Gilbert (LLG) equation which has a well-known Walker's exact rigid-body propagation solution [1] for a one-dimensional (1D) biaxial wire. This Walker solution plays a pivotal role [6–8] in our current understanding of both current-driven and field-driven DW propagation in magnetic nanowires. A genuine solution of a physical system must be stable against small perturbations. Although there is no proof of the stability of the Walker solution and there are signs [9, 10] that this solution may be unstable, at least under certain conditions, the validity of the Walker solution for a 1D wire is always taken as self-evident. Any deviation in experiments or numerical simulations are assumed to be attributed to the quasi-1D nature or other effects [7]. On the other hand, applications of spintronics devices require accurate description of DW motion [11–14]. Thus, the stability of the Walker propagating DW solution becomes vital in our understanding of DW propagation along a magnetic wire.

In this paper, by using a recipe that is based on a series of recent advances in nonlinear dynamics theory, the stability of the Walker's exact DW solution is theoretically analyzed. To our surprise, the solution is not stable against spin wave emission. In the low field region, only stern spin wave could be observed while both stern and bow waves emerge under high field. Severe distortion in propagating DW profile and resulted deviation of DW speed from the Walker formula can occur when the transverse magnetic anisotropy is larger than a critical value and the external field is sufficient high, but below the Walker breakdown field. For a given transverse magnetic anisotropy, the solution is transient unstable at low field and convective/absolute unstable at high field, corresponding to emitted different spin wavepackets.

To study the stability of Walker's exact propagating DW solution under an external field, we consider the di-

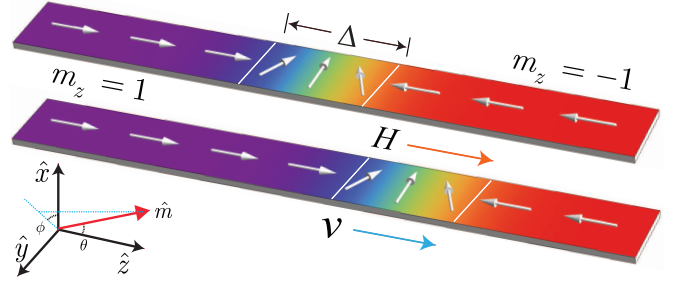


FIG. 1: (Color online) Illustration of transverse head-to-head DW of width Δ in a nanowire, with easy axis along \hat{z} and hard axis along \hat{x} . In the absence of external magnetic field (upper), a static DW exists between two domains with $m_z = \pm 1$. Under a field parallel to the easy axis, the Walker propagating DW moves towards the energy minimum state ($m_z = -1$) at a speed v while the DW profile is preserved.

mensionless 1D LLG equation [5],

$$\frac{\partial \vec{m}}{\partial t} = -\vec{m} \times \vec{h}_{eff} + \alpha \vec{m} \times \frac{\partial \vec{m}}{\partial t}. \quad (1)$$

This LLG equation describes the dynamics of magnetization \vec{M} of a magnetic nanowire schematically shown in Fig. 1. With the easy axis along the wire (\hat{z} direction) and the width and thickness being smaller than the exchange interaction length, exchange interaction dominates the stray field energy caused by magnetic charges on the edges; the DW structure tends to be homogeneous in the transverse direction [15], i.e., behaves effectively 1D. We are interested in the behavior of a head-to-head DW under an external field shown in Fig. 1. In Eq. (1), \vec{m} is the unit direction of the local magnetization $\vec{M} = \vec{m}M_s$ with saturation magnetization M_s and α is the phenomenological Gilbert damping constant. The effective field (in the units of M_s) is $\vec{h}_{eff} = K_{\parallel}m_z\hat{z} - K_{\perp}m_x\hat{x} + A\partial^2\vec{m}/\partial z^2 + H\hat{z}$ where K_{\parallel} , K_{\perp} , and A are respectively the easy axis anisotropy coefficient, the hard axis anisotropy coefficient, and the exchange coefficient. H is the external magnetic field parallel to \hat{z} . The time unit is $(\gamma M_s)^{-1}$, where γ is the gyromagnetic ratio. Using polar angle θ and azimuthal

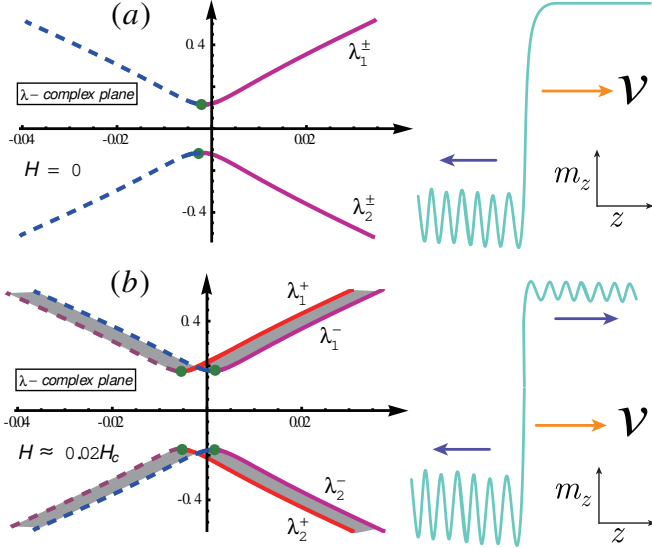


FIG. 2: (Color online) Left are the essential spectrum (shaded regions) for $H = 0$ (a) and $H \approx 0.02H_c$ (b). The Fredholm borders are $\lambda_{1,2}^{\pm}(k)$. Solid border lines correspond to spin waves with negative group velocities while the dashed border lines are for the spin waves with positive group velocities. Propagating DW wall emit stern waves in low fields (right of (a)), and stern and bow waves in higher field ($0.02H_c < H < H_c$) (right of (b)). The green dots are zero group velocity modes. $K_{\perp} = 1$ is used.

angle φ for \vec{m} as shown in Fig. 1, this LLG equation has a well known Walker propagating DW solution [1],

$$\sin 2\varphi_w(z, t) = \frac{H}{H_c}, \quad \ln \tan \frac{1}{2}\theta_w(z, t) = \frac{z - vt}{\Delta}. \quad (2)$$

Here $H_c = \alpha K_{\perp}/2$ is the Walker breakdown field and $\Delta = (K_{\parallel}/A + \cos^2\varphi_w K_{\perp}/A)^{-1/2}$ is the DW width which will be used as the length unit ($\Delta = 1$) in the analysis below. $v = \Delta H/\alpha$ is the Walker rigid-body DW speed that is linear in the external field and the DW width, and inversely proportional to the Gilbert damping constant. Solution (2) is exact for $H < H_c$.

To prove the instability of solution (2) against spin wave emission, we follow a recently developed theory (Sandstede, 2001 [16]; Fiedler and Scheel, 2003 [17]) for stability of a general travelling front such as a propagating head-to-head DW shown in Fig. 1. Consider a small deviation of the Walker solution, $\theta_w + \theta$ and $\varphi_w + \varphi$ with $|\theta| \ll 1$ and $|\varphi| \ll 1$, the equations satisfied by θ and φ can be readily obtained from Eq. (1). In the moving frame of the DW velocity v (with coordinate transformations of $z \rightarrow \xi \equiv z - vt$ and $t \rightarrow t$), the linearized equations of θ and φ in a two-component form of $\Lambda \equiv (\theta, \varphi)^T$ (superscript T means transpose) are

$$\frac{d\Lambda}{dt} = L(\theta_w, \varphi_w, \partial/\partial\xi, \partial^2/\partial\xi^2)\Lambda. \quad (3)$$

L is an inhomogeneous operator, depending on ξ through θ_w . The energy dissipation due to time variations of θ

and φ are absent because they are higher order terms [5]. It shall be important when the deviations are out of the linear regime. The possible solutions of Eq. (3) of type $\Lambda = \Lambda_1(\xi)e^{\lambda t}$ define spectrum Λ of L . Similar to energy spectrum of a quantum system, λ can be continuum and discrete. The former is often called essential spectrum while the later point spectrum. The spectrum λ shall determine the stability of the Walker solution. In terms of $\Lambda' \equiv (\theta, \varphi, \partial\theta/\partial\xi, \partial\varphi/\partial\xi)^T$, equation (3) becomes a four dimensional first-order ordinary differential system

$$\frac{d}{d\xi}\Lambda' = \Gamma\Lambda', \quad \Gamma = \begin{pmatrix} 0 & I \\ B & C \end{pmatrix}, \quad (4)$$

here I is a 2×2 identity matrix, and 2×2 matrices, B and C , have following matrix elements: $B_{11} = \alpha\lambda/A + (1/2A)(K_{\perp} - 2K_{\parallel} - K_{\perp}\sqrt{1-\rho^2})\cos[2G(\xi)] - H \tanh \xi/A$ where $G(\xi)$ is the Gudermannian function and $\rho = H/H_c$; $B_{12} = (\lambda - K_{\perp}\rho \tanh \xi)/(A \cosh \xi)$; $B_{21} = -\cosh \xi(2\lambda + K_{\perp}\rho \tanh \xi)/(2A)$; $B_{22} = (\alpha\lambda - K_{\perp}\sqrt{1-\rho^2})/A$; $C_{11} = -v\alpha/A$; $C_{12} = -v/(A \cosh \xi)$; $C_{21} = v \cosh \xi/A$; $C_{22} = -2 - v\alpha/A$.

According to the theory of Refs. [16–20], the spectrum of L is determined by Eq. (4). The essential spectrum is bordered by the Fredholm borders (defined below) of (4) with Γ replaced by its two limits of $\xi \rightarrow \pm\infty$, denoted as $\Gamma^{\pm} \equiv \lim_{\xi \rightarrow \pm\infty} \Gamma$. Since Γ^{\pm} are constant 4×4 matrices, solutions of Eq. (4) with $\Gamma = \Gamma^{\pm}$ are linear combinations of $\Lambda_0 e^{\kappa^{\pm}\xi}$ with κ^{\pm} being complex numbers. Pure plane wave solutions ($\kappa^{\pm} = ik$) exist only when λ satisfies $\det(\Gamma^{\pm}(\lambda) + ik) = 0$ with $k \in (-\infty, \infty)$. Each of the two equations has two branches of allowed λ labeled as $\lambda_{1,2}^{\pm}(k)$, known as the Fredholm borders [16, 17, 19]. In another word, Eq. (4) with $\Gamma = \Gamma^+$ ($\Gamma = \Gamma^-$) has pure plane wave solution when λ is on $\lambda_{1,2}^+(k)$ ($\lambda_{1,2}^-(k)$). For those λ not on $\lambda_{1,2}^{\pm}(k)$, each Eq. (4) with $\Gamma = \Gamma^{\pm}$ have four κ^{\pm} 's whose real parts are nonzero. If one uses $(n_{\pm}^{\pm}, n_{\mp}^{\pm})$ to denotes λ for n_{\pm}^{\pm} (n_{\mp}^{\pm}) being the number of κ^{\pm} 's with positive (negative) real part. Then both $\lambda_{1,2}^+(k)$ and $\lambda_{1,2}^-(k)$ divide λ -plane into three parts with $(n_{\pm}^{\pm}, n_{\mp}^{\pm}) = (1, 3)$, $(2, 2)$, and $(3, 1)$, respectively. According to theorem 5.35 in Chapter 4 of Kato [20], the essential spectrum of L must be in the regimes with $n_{\pm}^{\pm} + n_{\mp}^{\pm} \neq 4$. For λ on boundaries $\lambda_{1,2}^{\pm}$, the associated eigenmode is plane wave (spin wave) while eigenmodes for λ not on the boundaries are spin wavepackets.

In order to understand numerical results in Ref. [10], parameters of yttrium iron garnet (YIG) [14] are assumed in our analysis with $A = 3.84 \times 10^{-12} J/m$, $K_{\parallel} = 2 \times 10^3 J/m^3$, $\gamma = 35.1 kHz/(A/m)$, and $M_s = 1.94 \times 10^5 A/m$. $\alpha = 0.001$ is used and K_{\perp} is a varying parameter. Fig. 2 plots the essential spectrum for $K_{\perp} = 1$. In the absence of an external field, two branches of the spectrum of Γ^{\pm} are the same, $\lambda_{1,2}^+(k) = \lambda_{1,2}^-(k)$, shown in Fig. 2(a). Since the spectrum encroaches the right half plane, unstable plane waves shall exist and spin

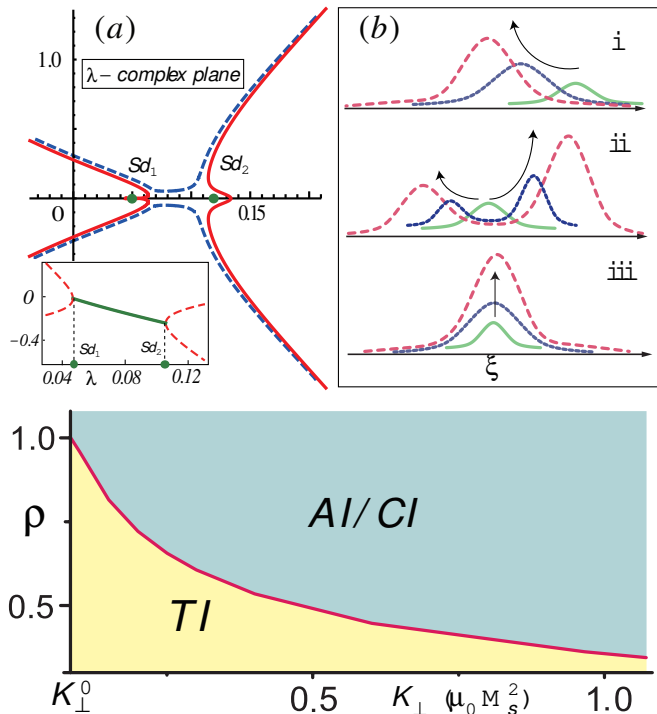


FIG. 3: (Color online) (a) $\lambda_{1,2}^-$ for $K_{\perp} = 1$, $\rho = 0.35$ (dashed curve) and 0.36 (solid curve). The absolute spectrum is between two branching points Sd_1 and Sd_2 (green dots). Inset: Plot of $Re(\kappa_2^-)$ and $Re(\kappa_3^-)$ vs. λ between Sd_1 and Sd_2 . At $Sd_{1,2}$, $\kappa_2^- = \kappa_3^-$. (b) Graphical illustrations of three types of instabilities caused by unstable absolute spectrum. Green curves indicate initial profiles of unstable modes while the dotted (blue) and dashed (red) curves are their later profiles. A transient instability (i) emits unidirectional waves (propagating to the left). A convective instability (ii) emits waves in both directions. An absolute instability (iii) emits waves that do not travel in the moving frame, or move with the DW. (c) Phase diagram of transient (TI) and absolute/convective (AI/CI) instabilities. The boundary is the bifurcation line between TI/CI-and-CI instabilities in K_{\perp} and $\rho = H/H_c$ plane. The bifurcation line is only plotted for $K_{\perp} \geq K_{\perp}^0$ here $K_{\perp}^0 \approx 0.085$ at which $H_2 = H_c$ ($\rho = 1$). Noted that our analysis is valid for fields below the Walker breakdown value.

wave emission are expected. Similar conclusion was also obtained in early study [21]. Solid lines are for negative group velocity (determined by $Im(\partial\lambda/\partial k)$), thus these are stern modes. The dashed lines indicate positive group velocity, corresponding to bow modes. The green dots are zero group velocity points. According to Fig. 2(a), all unstable modes have negative group velocities so that DW can only emit stern waves in the low fields. As the external field increases, $\lambda_{1,2}^+(k)$ and $\lambda_{1,2}^-(k)$ are different, and the area of essential spectrum in λ -plane becomes bigger and bigger (shadowed regimes in Fig. 2(b)). The green dots also moves toward $Im(\lambda)$ -axis and cross it at $H \approx 0.02H_c$ (Fig. 2(b)). Further increase of H , the unstable modes have both positive and negative group velocities although the most of them have the negative ones. One shall have propagating DW to emit both stern

and bow waves. The stern waves should be stronger than the bow waves as schematically shown in the right figure of Fig. 2(b). This is exactly what were observed in numerical simulations on dissipative wires for stern wave emission in low field [9] and stern-and-bow wave emission in high field [10]. In a realistic wire with damping, emitted spin waves will be dissipated after a short distance, and are hard to be observed in experiments.

Interestingly, severe instabilities of a propagating DW are not determined by the essential spectrum, but by the absolute spectrum [16–20, 22–24] that could change the DW profile so that DW propagating speed would be substantially modified [5]. As mentioned early, for each λ in the complex plane, there are four κ_i^{\pm} ($i = 1, 2, 3, 4$) for Γ^{\pm} , ordered by their real parts as $Re(\kappa_1^{\pm}) \geq Re(\kappa_2^{\pm}) \geq Re(\kappa_3^{\pm}) \geq Re(\kappa_4^{\pm})$. Then λ is said to belong to the absolute spectrum if and only if $Re(\kappa_2^+(\lambda)) = Re(\kappa_3^+(\lambda))$ or $Re(\kappa_2^-(\lambda)) = Re(\kappa_3^-(\lambda))$ [24, 27]. The branching points are special points in the absolute spectrum, denoted as λ_{sd} , satisfying $\kappa_2^{\pm}(\lambda_{sd}) = \kappa_3^{\pm}(\lambda_{sd})$. They are non-traveling modes [24, 27]. For $K_{\perp} = 1$, the absolute spectrum in the right half λ -plane is generated by Γ^- . Fig. 3(a) shows two branches $\lambda_{1,2}^-$. They are well separated by the real axis for $\rho = 0.35$ as shown in Fig. 3(a) (dashed curves) and no absolute spectrum could be found in the right half plane. As the field increases, the two branches get closer with each other and at an onset field H_2 , depending on K_{\perp} , two branches tangent at the real axis and then separate again in horizontal direction as shown in Fig. 3(a) for $\rho = 0.36$ (solid curves). At this moment, the absolute spectrum begin to emerge on the real axis (the segment between two branching points $Sd_{1,2}$ (green solid dots)). The dependence of $Re(\kappa_2^-)$ or $Re(\kappa_3^-)$ on $Re(\lambda)$ between these two points is shown in the inset of Fig. 3(a) (solid segment).

According to Refs. [22–24], wavepackets would be emitted if the essential spectrum encroaches the right half λ -plane. There are three types of instability [16–19, 22–24]. The instability is called transient (TI) if the essential spectrum encroaches the right half plane and absolute spectrum are either in the left half plane or does not exist. The propagating DW emits stern waves shown in Fig. 3(b)i. The instability is called convective if both essential and absolute spectrum encroaches the right half λ -plane. In this case, the emitted waves can propagate in both direction as shown by Fig. 3(b)ii. For a convective instability, if any branching point is also in the right half λ -plane, the instability is called absolute. An absolute instability can then emit non-traveling (zero group velocity) waves as illustrated in Fig. 3(b)iii. For LLG equation, since the absolute spectrum is the segment connecting two branching points Sd_1 and Sd_2 (Fig. 3 (a)), the absolute instability (AI) and convective instability (CI) co-exist. It is known that transient instability is very weak that can be removed under proper mathematical treatment [16, 26]. Thus, we should not expect to

have great physical consequences. On the other hand, the absolute instability move with the DW, and cause the change of DW profile [24–26]. It is known [5] that field-induced DW propagating speed is proportional to the energy damping rate that is sensitive to DW profile. Therefore absolute instability, which deform propagating DW profile, shall substantially alter DW speed. This may explain why the field-induced DW speed start to deviate from the Walker result only when the field is large enough to emit both stern and bow waves in simulations [10].

Fig. 3(c) is the calculated phase diagram in K_{\perp} and $\rho = H/H_c$ plane. A transition from transient instability (denoted as TI in the figure) to absolute/convective instability (AI/CI) occur at a critical field H_2 as lng as $K_{\perp} > K_{\perp}^0 \approx 0.085$ at which $H_2 = H_c$. It means no absolute/convective instability exist for $K_{\perp} < K_{\perp}^0$, and one shall not see noticeable change in famous Walker propagation speed mentioned early. This may explain why many previous numerical simulations on permalloy, which have small transverse magnetic anisotropy, are consistent with Walker formula. A snapshot of the convecting wavepackets could be identified in Fig. 2 in Reference [10] where wavepackets can be seen in the vicinity of the traveling DW and travel to both directions.

It should be noticed that the effects of point spectrum have not been analyzed. In principle, it can also affect the stability of the Walker solution, and should be a very interesting subject too. Unfortunately, there are not many theorems on the point spectrum yet. Thus, one can only rely on a numerical method to find a point spectrum of operator L and to find out whether it can also induce any instability on a propagating DW.

In conclusion, we showed that a Walker propagating DW will always emit stern waves in a low field, and both stern and bow waves in a higher field. Thus the exact Walker solution of LLG equation is not stable. The true propagating DW is always dressed with spin waves. The emitted spin waves shall be damped away during their propagation, and make them hard to be detected in realistic wires. For a realistic wire with its transverse magnetic anisotropy larger than a critical value and when the applied external field is larger than certain value, a propagating DW may undergo simultaneous convective and absolute instabilities. As a consequence, the propagating DW will not only emit both spin waves and spin wavepackets, but also change significantly its profile. Thus, the corresponding Walker DW propagating speed will deviate from its predicted value, agreeing very well with recent simulations.

This work is supported by Hong Kong RGC Grants (604109 and RPC11SC05).

- [1] N.L. Schryer and L.R. Walker, J. Appl. Phys. **45**, 5406 (1974).
- [2] S.S.P. Parkin, M. Hayashi, and L. Thomas, Science **320**, 190 (2008).
- [3] D.A. Allwood, G. Xiong, C.C. Faulkner, D. Atkinson, D. Petit, and R.P. Cowburn, Science **309**, 1688 (2005).
- [4] G.S.D. Beach, C. Knutson, C. Nistor, M. Tsoi, and J.L. Erskine, Phys. Rev. Lett. **97**, 057203 (2006).
- [5] X.R. Wang, P. Yan, J. Lu and C. He, Ann. Phys. (N.Y.) **324**, 1815 (2009); X.R. Wang, P. Yan, and J. Lu, EPL **86**, 67001 (2009).
- [6] Z. Li and S. Zhang, Phys. Rev. Lett. **92**, 207203 (2004).
- [7] A. Thiaville1, S. Rohart, Ju.V. Cros and A. Fert, EPL **100**, 57002 (2012).
- [8] J. Linder, Phys. Rev. B **87**, 054434 (2013).
- [9] R. Wieser, E.Y. Vedmedenko, and R. Wiesendanger, Phys. Rev. B **81**, 024405 (2010).
- [10] X.S. Wang, P. Yan, Y.H. Shen, G.E.W. Bauer, and X.R. Wang, Phys. Rev. Lett. **109**, 167209 (2012).
- [11] J. Stöhr and H.C. Siegmann, *Magnetism: From Fundamentals to Nanoscale Dynamics*, (Springer-Verlag, Berlin, 2006).
- [12] M. Hatami, G.E.W. Bauer, Q. Zhang, and P.J. Kelly, Phys. Rev. Lett. **99**, 066603 (2007).
- [13] D.S. Han, S.K. Kim, J.Y. Lee, S.J. Hermsdoerfer, H. Schultheiss, B. Leven, and B. Hillebrands, Appl. Phys. Lett. **94**, 112502 (2009).
- [14] P. Yan, X.S. Wang, and X.R. Wang, Phys. Rev. Lett. **107**, 177207 (2011).
- [15] D.G. Porter and M.J. Donahue, J. Appl. Phys. **95**, 6729 (2004).
- [16] B. Sandstede and A. Scheel, Dynam. Syst. **16**, 1 (2001); B. Sandstede, and A. Scheel, Math. Nachr. **232**, 39 (2001).
- [17] B. Fiedler and A. Scheel, in *Trends in Nonlinear Analysis*, edited by M. Kirkilionis, S. Kromker, R. Rannacher, and F. Toni (Springer, 2003).
- [18] D. Henry, *Geometric Theory of Semilinear Parabolic Equations*, (Springer, 1981).
- [19] K.J. Palmer, Proc. Am. Math. Soc. **104**, 149 (1988).
- [20] L. Perko, *Differential Equations and Dynamical Systems*, (Springer, 2001); T. Kato, *Perturbation Theory for Linear Operators*, (Springer, 1995).
- [21] D. Bouzidi and H. Suhl, Phys. Rev. Lett. **65**, 2587 (1990).
- [22] J.M. Chomaz, Phys. Rev. Lett. **69**, 1931 (1992); A. Couairon, and J.M. Chomaz, Physica D **108**, 236 (1997).
- [23] L. Brevdo and T. J. Bridges, Philos. Trans. R. Soc. London, Ser. A **354**, 1027 (1996).
- [24] B. Sandstede, *Handbook of Dynamical Systems II*, (North-Holland, 2002); B. Sandstede and A. Scheel, Phys. Rev. E. **62**, 7708 (2000).
- [25] R.L. Pego and M.I. Weinstein, Commun. Math. Phys. **164**, 305 (1994).
- [26] J. Humpherys, B. Sandstede, and K. Zumbrun, Numer. Math. **103**, 631 (2006); J. Humpherys and K. Zumbrun, Physica D **220**, 116 (2006).
- [27] J.D.M. Rademacher, J. Appl. Dyn. Syst. **5**, 634 (2006)

* Electronic address: [Corresponding author:]phxwan@ust.hk